Effect of Time-Interleaved Analog-to-Digital Converter Mismatches on OFDM Performance

Vo-Trung-Dung Huynh[1], Nele Noels[1], Pieter Rombouts[2], Jean Armstrong[3], Heidi Steendam[1]
[1]Department of Telecommunications and Information Processing, Ghent University
[2]Department of Electronics and Information Systems, Ghent University
[3]Department of Electrical and Computer Systems Engineering, Monash University
[1]{votrungdung.huynh, nele.noels, heidi.steendam}@telin.ugent.be
[2]{pieter.rombouts}@elis.ugent.be
[3]{jean.armstrong}@monash.edu

***Abstract*— For the extremely high sampling rate and high resolution required for multi-Gigabit orthogonal frequency division multiplexing (OFDM) communication systems, time-interleaved analog-to-digital converters (ADCs) are being considered. However, in practice, mismatches such as offset mismatch, gain mismatch and timing mismatch occur between the parallel sub-ADCs. This paper theoretically analyzes the impact of the different mismatches on the performance of the OFDM system. The theoretical results are confirmed by simulations and show that OFDM performance is strongly degraded, even for small mismatches.**

***Index Terms*— OFDM, time-interleaved analog-to-digital converter, mismatch, performance.**

I. Introduction

Orthogonal frequency division multiplexing (OFDM) is an efficient multi-carrier transmission technique that is widely adopted in many wired and wireless standards, thanks to its high spectral efficiency, inherent bandwidth management and tolerance against channel dispersion. In the last decade, it has also been suggested for multi-Gigabit fiber-optic communication systems [1]. In such a high-speed OFDM system, the trend is to minimize the number of analog components in favour of digital signal processing (DSP). As a result, the analog-to-digital converter is placed prior to the baseband DSP core, implying the ADC needs to operate at an extremely high sampling rate. Current devices are not able to meet the requirements as they are already operating close to the physical limits of the used technology [2]. As a result, the increase in speed in the coming years is expected to be rather modest. A low cost solution to this hardware restriction is the use of time-interleaved ADCs (TI-ADCs) [3].

In a TI-ADC architecture, L slow sub-ADCs are placed in parallel, as shown in Fig. 1. The l^{th} ADC slicer samples the signal at instant CK_l, $l = 0, ..., L-1$, where the sampling instants are shifted in time. Ideally, these sampling instants are equidistant with as spacing the sampling time T_s. In this way, the overall sampling rate is L times higher than the sampling rate $\frac{1}{LT_s}$ of each sub-ADC. However, mismatches between the parallel sub-ADCs, such as offset and gain mismatch as well as the time skew of the used clocks in the sub-ADCs, can degrade the performance of the TI-ADC. Although there are a few authors that have studied the effects of TI-ADC mismatches on high-rate OFDM systems, their results are based on simulations only [2], [4]. There is also some closely related work on the effect of timing jitter in OFDM systems [5], [6]. In this paper, we evaluate the effects of these mismatches in an analytical way. The theoretical results, which are in agreement with our simulation results, can be used for deriving calibration methods for TI-ADCs used in high-speed OFDM-based systems.

The paper is organized as follows. In Section II, we describe the system model, including the model of the OFDM transceiver and the model of the TI-ADC with the offset, gain and timing mismatch. In order to assess the bit error rate (BER) performance of the OFDM system, a theoretical analysis of the effect of these mismatches on the spectrum of the sampled OFDM signal and on the output of the discrete Fourier transform (DFT) unit that is used to demodulate the resulting samples is presented in Section III and Section IV, respectively. In Section V, we first validate the accuracy of the derived expressions by comparing the theoretical results with the simulation results, and then we numerically assess the effects of the TI-ADC mismatches on the BER performance of the system. Finally, our conclusion is given in Section VI.

II. System Model

In this section, we describe the considered OFDM transceiver model, of which the system block diagram is provided in Fig. 2. The receiver is assumed to employ a TI-ADC architecture in which the different sub-ADCs experience different offset, gain and timing mismatches. The model of the l^{th} sub-ADC of the TI-ADC, with offset (do_l), gain (dg_l) and timing (dt_l) mismatch is illustrated in Fig. 1 [7]. Since the mismatch parameters vary slowly over time, we can model them as constants over the duration of an OFDM symbol period.

In an OFDM-based system with N sub-carriers, a high-rate data stream is divided into N parallel low-rate data streams, which are modulated on the different sub-carriers

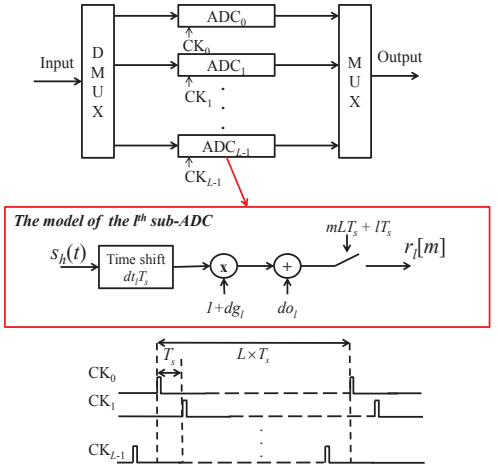

Fig. 1. Block diagram of the TI-ADC and the model of the mismatches in the l^{th} sub-ADCs.

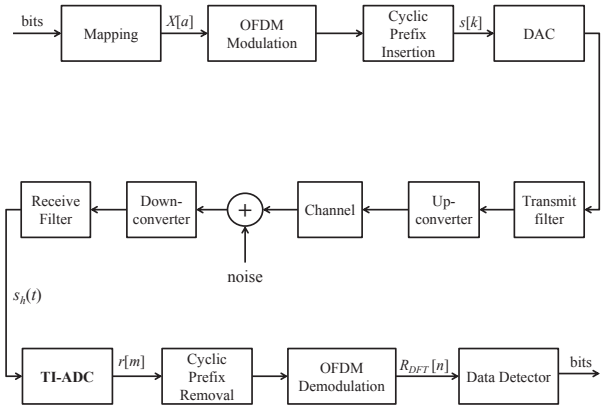

Fig. 2. Block diagram of a OFDM system with a TI-ADC at receiver.

with an inverse discrete Fourier transform (IDFT). Let the vector $\boldsymbol{X}$ denote the input of the IDFT. Then, the vector $\boldsymbol{X}$ consists of N complex-valued symbols (i.e., $\boldsymbol{X}$ = ($X[0]$, $X[1]$,..., $X[N\text{-}1]$)^t, where the superscript t denotes transpose), which are taken from an M-ary Phase Shift Keying (PSK) or Quadrature Amplitude Modulation (QAM) constellation with each constellation symbol corresponding to a sequence of $\log_2(M)$ bits. The IDFT converts the data symbols to the time domain. Because of channel dispersion, the pulses assigned to the time-domain samples will be spread in time. In order to avoid inter-symbol interference (ISI) at the receiver, which causes a performance degradation, adjacent OFDM symbols are separated by a guard interval. In this paper, the guard interval consists of a cyclic prefix (CP), where the last samples of each OFDM symbol are copied and placed in front of the samples generated by the IDFT. The time-domain samples of an OFDM symbol after CP insertion are given by:

$$s[k] = \sum_{a=0}^{N-1} X[a] e^{j2\pi \frac{ak}{N}}, \quad -N_{CP} \leq k \leq N-1, \quad (1)$$

where N_{CP} is the number of cyclic prefix samples. The digital-to-analog converter (DAC) converts the discrete-time OFDM sequence (1) to a continuous-time signal by using pulses spaced by an interval T_s. The resulting signal is shaped by the transmit filter, and up-converted from the baseband to the high frequency of the carrier, in order to transmit the signal over the channel.

At the receiver, the received waveform is down-converted, passed through a receive filter and sampled at Nyquist rate $\frac{1}{T_s}$ by a TI-ADC. The signal $s_h(t)$, which is the input of the TI-ADC, can be expressed as:

$$s_h(t) = \sum_{k=-\infty}^{+\infty} s[k] h_{eq}(t - kT_s) + noise, \quad (2)$$

where $s[k]$ is defined by (1) and $h_{eq}(t)$ is the equivalent impulse response of the cascade of the transmit filter, the channel and the receive filter. It is assumed that the duration of $h_{eq}(t)$ is restricted to the interval $[0, N_{CP}T_s]$ such that no ISI occurs. To simplify the notations, we consider the transmission of only one OFDM symbol and neglect other OFDM symbols transmitted in different time intervals. In that case, the output of the TI-ADC given in Fig. 1, can be written as:

$$r[m] = \sum_{l=0}^{L-1} \sum_{q=-\infty}^{+\infty} \delta[m - qL - l] \cdot ((1 + dg_l) \cdot s_h[m - dt_l] + do_l) + noise, \quad m = -N_{CP}, ..., N-1, \quad (3)$$

where $r[m]$ denotes the m^{th} sample, $s_h[.]$ is defined as $s_h[m] = s_h(mT_s)$ and $\delta[.]$ denotes the discrete dirac function. After removing the cyclic prefix, the samples $r[m]$, $m = 0, ..., N-1$, from (3) are applied to a discrete Fourier transform (DFT). The signal at the output of the DFT unit can be written as:

$$R_{DFT}[n] = \frac{1}{N} \sum_{m=0}^{N-1} r[m] e^{-j2\pi \frac{mn}{N}}, \quad n = 0, 1, ..., N-1. \quad (4)$$

The quantities $R_{DFT}[n]$ are used to perform symbol detection, after which estimates of the information bits are computed by e.g. applying the inverse of the mapping rule.

To simplify the notational complexity in our analysis, we assume that the number of sub-ADCs is a power of two. However, the extension to other values of L is straightforward.

III. Analysis of Mismatch Effects on OFDM Spectrum

In the literature, the effect of the TI-ADC mismatches on (single-carrier) communication systems is commonly investigated by evaluating the spectral behavior after the TI-ADC. Therefore, in this section, we consider the effect of the mismatches on the spectrum of the OFDM signal. To this end, we consider the power spectral density (PSD) after the TI-ADC, but in front of the DFT. The PSD is approximated by taking the averaged modulo-square

of the frequency response of the signal. Neglecting the presence of the noise, the frequency response of $r[m]$, $m = 0, ..., N-1$ defined in (3), is found to be:

$$\begin{aligned} R_{\text{joint}}(f) &= \sum_{m=-N_{CP}}^{N-1} r[m] \cdot e^{-j2\pi fm} \\ &= \sum_{l=0}^{L-1} \left((1+dg_l) \cdot S_h(f) \cdot e^{-j2\pi f dt_l} \otimes D_l(f)\right) \\ &+ \sum_{l=0}^{L-1} do_l \cdot D_l(f), \end{aligned} \tag{5}$$

where $\otimes$ denotes convolution, $S_h(f)$ is the frequency response of $s_h[m]$ given by:

$$S_h(f) = \sum_{m=-N_{CP}}^{N-1} s_h[m] \cdot e^{-j2\pi fm}, \tag{6}$$

and $D_l(f)$ is the frequency response of an infinite sum of dirac functions defined as:

$$\begin{aligned} D_l(f) &= \sum_{m=-N_{CP}}^{N-1} \sum_{q=-\infty}^{+\infty} \delta[m - qL - l] \cdot e^{-j2\pi fm} \\ &= \tfrac{1}{L} \sum_{i=-\infty}^{+\infty} \delta(f - \tfrac{i}{LT_s}) \cdot e^{-j\frac{2\pi i}{L}l}. \end{aligned} \tag{7}$$

Substituting (7) into (5), the frequency response of the output of the TI-ADC including all mismatches is given by:

$$\begin{aligned} R_{\text{joint}}(f) = &\sum_{i=-\infty}^{+\infty} DGT_i(f) \cdot S_h(f - \tfrac{i}{LT_s}) \\ &+ \sum_{i=-\infty}^{+\infty} DO_i \cdot \delta(f - \tfrac{i}{LT_s}), \end{aligned} \tag{8}$$

where $DGT_i(f)$ and DO_i are given by:

$$DGT_i(f) = \frac{1}{L} \sum_{l=0}^{L-1} (1+dg_l) \cdot e^{-j2\pi(f - \frac{i}{LT_s})dt_l} \cdot e^{-j\frac{2\pi i}{L}l}, \tag{9}$$

$$DO_i = \frac{1}{L} \sum_{l=0}^{L-1} do_l \cdot e^{-j\frac{2\pi i}{L}l}. \tag{10}$$

Next, we separately consider the effect of the different mismatches on the PSD to clearly isolate the influence of each mismatch.

• ***Offset Mismatch:*** In this case, we consider the effect caused by the offset mismatch do_l only. The other mismatches are neglected, i.e., $dg_l = 0$ and $dt_l = 0$. The frequency response of $r[m]$ in (3) becomes:

$$R_{\text{offset}}(f) = \sum_{i=-\infty}^{+\infty} S_h(f - \frac{i}{T_s}) + \sum_{i=-\infty}^{+\infty} DO_i \cdot \delta(f - \frac{i}{LT_s}), \tag{11}$$

where we used:

$$\frac{1}{L} \sum_{l=0}^{L-1} e^{-j\frac{2\pi i}{L}l} = \begin{cases} 1, & \text{if } \frac{i}{L} \text{ is integer} \\ 0, & \text{else} \end{cases}. \tag{12}$$

• ***Gain Mismatch:*** Similarly, if the offset and timing mismatch are ignored, i.e., $do_l = 0$ and $dt_l = 0$, the frequency response of $r[m]$ in the presence of the gain mismatch dg_l is given by:

$$R_{\text{gain}}(f) = \sum_{i=-\infty}^{+\infty} S_h(f - \frac{i}{T_s}) + \sum_{i=-\infty}^{+\infty} DG_i \cdot S_h(f - \frac{i}{LT_s}), \tag{13}$$

where DG_i is given by:

$$DG_i = \frac{1}{L} \sum_{l=0}^{L-1} dg_l \cdot e^{-j\frac{2\pi i}{L}l}. \tag{14}$$

• ***Timing Mismatch:*** In this case, only the timing mismatch dt_l is present and the other mismatches are not taken into account. The frequency response of $r[m]$ can be expressed as:

$$R_{\text{timing}}(f) = \sum_{i=-\infty}^{+\infty} DT_i(f) \cdot S_h(f - \frac{i}{LT_s}), \tag{15}$$

where $DT_i(f)$ is given by:

$$DT_i(f) = \frac{1}{L} \sum_{l=0}^{L-1} e^{-j2\pi(f - \frac{i}{LT_s})dt_l} \cdot e^{-j\frac{2\pi i}{L}l}. \tag{16}$$

From (11), it can be observed that offset mismatch causes the introduction of data-independent tones at frequencies $\frac{i}{LT_s}$ in the spectrum, whereas (13) indicates that the gain mismatch produces replicas of the main OFDM spectrum, weighted by DG_i and shifted by $\frac{i}{LT_s}$. Furthermore, from (15), it follows that the timing mismatch has a similar effect on the OFDM spectrum as the gain mismatch, but additionally, the main spectrum and replica spectra are distorted due to the frequency-dependent phase shift $DT_i(f)$ caused by the timing skew, as indicated in (16).

IV. Analysis of Mismatch Effects on DFT Output

In the section with the numerical results, we will show that the performance of the OFDM system in the presence of the mismatches is difficult to evaluate based on the spectrum only. Therefore, in this section, we evaluate the impact of the mismatches caused by the TI-ADC on the OFDM signal at the DFT output in order to assess the influence of these mismatches on the BER performance. Substituting (3) into (4) and neglecting the presence of the noise, we obtain:

$$\begin{aligned} R_{\text{DFT-joint}}[n] = &\tfrac{1}{N} \sum_{m=0}^{N-1} \sum_{l=0}^{L-1} \sum_{q=-\infty}^{+\infty} \delta[m - qL - l] \cdot \\ &\left((1+dg_l) \sum_{k=-\infty}^{+\infty} h_{eq}[k] s[m-k-dt_l] + do_l\right) \cdot e^{-j2\pi\frac{mn}{N}}, \\ &n = 0, 1, ..., N-1. \end{aligned} \tag{17}$$

Let us define $H_{eq}[.]$ as the channel frequency response:

$$H_{eq}[a] = \sum_{k=-\infty}^{+\infty} h_{eq}[k] \cdot e^{-j2\pi\frac{ka}{N}}, \quad a = 0, 1, ..., N-1. \tag{18}$$

Taking into account (18) and (1), the DFT output (17) can be written as:

$$\begin{aligned} R_{\mathrm{DFT-joint}}[n] &= \sum_{i=0}^{L-1}\sum_{l=0}^{L-1} \\ &\left(\tfrac{1+dg_l}{L}\right)\sum_{a=0}^{N-1} H_{eq}[a]\cdot X[a]\cdot e^{-j2\pi\frac{adt_l}{N}}\cdot \delta\left[a-n+\tfrac{i}{L}N\right] \\ &+\sum_{i=0}^{L-1}\sum_{l=0}^{L-1}\tfrac{do_l}{L}\cdot e^{-j\frac{2\pi i}{L}l}\cdot\delta\left[n-\tfrac{i}{L}N\right] \\ &=\sum_{i=0}^{L-1} DGT_i(\tfrac{n}{NT_s})\cdot H_{eq}[n-\tfrac{i}{L}N]\cdot X[n-\tfrac{i}{L}N] \\ &+\sum_{i=0}^{L-1} DO_i\cdot\delta[n-\tfrac{i}{L}N], \qquad n=0,1,...,N-1, \end{aligned} \tag{19}$$

where $DGT_i(.)$ and DO_i are defined in (9) and (10), respectively.

To better understand the effect of each mismatch on the BER performance, we will separately discuss the influence of each mismatch on the DFT output required to detect the data symbols.

• ***Offset Mismatch:*** In this case, the offset mismatch do_l is present and the other mismatches are neglected. The DFT output can be expressed as:

$$\begin{aligned} &R_{\mathrm{DFT-offset}}[n] = \\ &\sum_{i=0}^{L-1}\sum_{l=0}^{L-1}\tfrac{1}{L}\cdot e^{-j\frac{2\pi i}{L}l}\cdot H_{eq}[n-\tfrac{i}{L}N]\cdot X[n-\tfrac{i}{L}N] \\ &+\sum_{i=0}^{L-1} DO_i\cdot\delta[n-\tfrac{i}{L}N], \qquad n=0,1,...,N-1. \end{aligned} \tag{20}$$

Substituting (12) into (20), the DFT output becomes:

$$R_{\mathrm{DFT-offset}}[n] = H_{eq}[n]X[n] + \sum_{i=0}^{L-1} DO_i\cdot\delta[n-\tfrac{i}{L}N], \quad n=0,1,...,N-1, \tag{21}$$

where DO_i is defined in (10).

• ***Gain Mismatch:*** Similarly, the DFT output with the influence of the gain mismatch dg_l can be expressed as:

$$\begin{aligned} R_{\mathrm{DFT-gain}}[n] &= H_{eq}[n]X[n] \\ &+\sum_{i=0}^{L-1} DG_i H_{eq}[n-\tfrac{i}{L}N]X[n-\tfrac{i}{L}N], \\ &\qquad n=0,1,...,N-1, \end{aligned} \tag{22}$$

where DG_i is defined in (14).

• ***Timing Mismatch:*** In the presence of the timing mismatch dt_l, the DFT output is given by:

$$\begin{aligned} &R_{\mathrm{DFT-timing}}[n] = \\ &\sum_{i=0}^{L-1} DT_i(\tfrac{n}{NT_s})H_{eq}[n-\tfrac{i}{L}N]X[n-\tfrac{i}{L}N], \\ &\qquad n=0,1,...,N-1, \end{aligned} \tag{23}$$

where $DT_i(.)$ is defined in (16).

As expected from Section III, the offset mismatch introduces complex-valued data-independent peaks to the sub-carriers at positions $\frac{i}{L}N$ and a real-valued peak at frequency 0 (see (21) and (11)). Taking into account that the data symbol transmitted on these sub-carriers are complex-valued, both the real and imaginary part of these data symbols are affected by the offset mismatch. Hence, for large signal-to-noise ratios (SNR) and sufficiently large values of the offset mismatch, we expect an error floor in the BER performance. This error floor can be approximated by:

$$\begin{aligned} \mathrm{BER}_{\mathrm{offset}} \approx{}& \Pr[\text{no peak}]\cdot\mathrm{BER}[\text{no peak}] \\ &+\Pr[\text{peak}]\cdot\mathrm{BER}[\text{peak}], \end{aligned} \tag{24}$$

where $\Pr[\text{peak}] = 1-\Pr[\text{no peak}]$ and $\Pr[\text{peak}] = \frac{L_1}{N}$ is the probability that a sub-carrier is affected by a peak introduced by the offset mismatch, with $L_1 \le L$[1] is the number of peaks occurring in the data-bearing part of the DFT output. The probability BER[no peak] corresponds to the BER of the OFDM system as if no mismatch is present, while BER[peak] is the probability of a bit error if the carrier is affected by the offset mismatch. In the worst case, when this offset is large, on average half of the bits of the data symbols will be erroneous. Hence, BER[peak] can be approximated by $\frac{1}{2}$ for the sub-carriers $\frac{i}{L}N$ ($i\neq 0$) and $\frac{1}{4}$ for $i=0$, where only the real part of the symbol is affected. This results in the BER:

$$\mathrm{BER}_{\mathrm{offset}} \approx (1-\frac{L_1}{N})\cdot\mathrm{BER}_{\mathrm{no\,mismatch}} + \frac{L_1-1}{2N} + \frac{1}{4N}. \tag{25}$$

A similar analysis for the gain mismatch and the timing mismatch turns out to be more complex. However, (22) and (23) indicate that all sub-carriers are affected by the gain and timing mismatch, which could also be expected from the spectral contents given in (13) and (15). Taking into account that all sub-carriers are disturbed by an interference term, which originates from other data symbols and is proportional to the number of sub-ADCs and the levels of the mismatches, it is expected that the BER will significantly increase with the number of sub-ADCs. Furthermore, if the interference term becomes the dominating contribution, the BER will show an error floor, which will become apparent at large SNR.

V. Numerical Results

In this section, we first investigate the validity of the proposed expressions for the spectral behavior by comparing the theoretical approximations for the PSD with simulations. To illustrate the results, we use the European Digital Video Broadcasting-Terrestrial (DVB-T) 2k mode standard [8] as the PHY protocol. We consider an OFDM signal containing 1705 data carriers and 343 unused carriers for the guard band; each of the data carriers is modulated with symbols drawn from the 4-QAM constellation. The transmit and receive filter are a 13^{th}-order Butterworth lowpass filter with a roll-off factor of $\frac{1}{14}$. In the following, we assume that the values of the mismatches are fixed. To obtain these reference values, we selected them uniformly in the intervals $[-\frac{A_o}{10};\frac{A_o}{10}]$ for the offset mismatch and $[-\frac{1}{10};\frac{1}{10}]$ for the gain and timing

[1]In case not all sub-carriers are modulated, some of the peaks occurring in the spectrum at positions $\frac{i}{L}N$ will not coincide with a data-bearing sub-carrier. Hence, the number L_1 of sub-carriers affected by a peak is upper bounded by L.

mismatch, respectively. Here, A_0 corresponds to the root-mean-square (RMS) amplitude value of the TI-ADC input $s_h(t)$, defined as:

$$A_o = \lim_{T\to\infty} \sqrt{\frac{1}{T}\int_0^T (s_h(t))^2 dt}. \quad (26)$$

These intervals correspond to 10% of the signal amplitude (for the offset and gain mismatch) and the Nyquist sampling rate $\frac{1}{T_s}$ (for the timing mismatch), respectively. The selected reference values used throughout this section are given in Table I.

TABLE I
MISMATCH PARAMETERS

Mismatches	Reference values
Offset ($\frac{do_l}{A_0}$)	$\frac{1}{100}\times$[1.6, 1.2, -5.9, -1.2, 3.1, -6.6, 4.1, -9.4]
Gain (dg_l)	$\frac{1}{100}\times$[3.3, -2.4, -0.95, -7.3, 4.85, -9.23, -5.9, 2.1]
Timing (dt_l)	$\frac{1}{100}\times$[-2,2, 1.5, -1.1, 4.4, 3.9, -5.1, 6.2, 1.6]

To isolate the effect of the TI-ADC mismatches on the OFDM spectrum, we consider an ideal channel. Fig. 3 illustrates the theoretical spectra from Section III as well as the simulated spectra based on Welch's periodogram [9]. It is assumed that the number L of sub-ADCs is equal to 4. The mismatch values are fixed and given by the first four values for each mismatch indicated in Table I. Fig. 3 shows that the simulation results closely approach the theoretical results, which demonstrates the accuracy of the derived expressions. From Fig. 3, as expected, it can be seen that the offset mismatch causes peaks in the OFDM spectrum at frequencies $\frac{i}{LT_s}$ with i = [-2,-1,0,1,2]. Furthermore, at first sight, the effect of the gain mismatch on the spectrum is small. The addition of the replicas of the main spectrum, centered around the frequencies $\frac{i}{LT_s}$ with i = [-2,-1,0,1,2] and weighted by DG_i (14), only introduces small variations in the spectrum compared to the case of no mismatch. Although the effect of the timing mismatch is similar to that of the gain mismatch, i.e. copies of the main spectrum centered around the frequencies $\frac{i}{LT_s}$, and additionally distorted by $DT_i(f)$ (16), the effect of the timing mismatch is better visible in the spectrum, especially in the center of the frequency band. Combining all three effects, in Fig. 3d, mainly the effects of the offset mismatch and the timing mismatch are visible. However, although at first sight, the gain mismatch and timing mismatch have only small effect on the spectrum of OFDM at the output of the TI-ADC, we will see later in this section, when evaluating the outputs of the DFT and the corresponding BER curves, that the gain and timing mismatch will have a larger influence on the OFDM performance than the offset mismatch, mainly because more sub-carriers are affected. Hence, the spectrum at the TI-ADC output, which is commonly used in the literature to evaluate the effect of the mismatches, turns out to be not effective in OFDM applications. Therefore, we will have to resort to the analysis of the DFT output and the BER results.

Fig. 4 compares the real and imaginary part of the DFT output obtained with the expressions (19)-(23) and through simulations. Again, Fig. 4 shows that the simulation results are close to the theoretical results, which illustrates the accuracy of the proposed expressions. As expected, the offset mismatch causes complex-valued peaks at the $\frac{i}{L}N$-index sub-carriers ($i \neq 0$) and a real-valued peak at the 0^{th} sub-carrier. For large offsets, we pointed out in Section IV that the offset mismatch would lead to an error floor in the BER curve at high SNR. In our example, where L_1 = 3, the error floor from (25) is expected to be approximately 7.4x10^{-4}. Furthermore, in Fig. 4b and Fig. 4c, it can be observed that the gain and timing mismatch equally affects the real and imaginary parts of the DFT output, although in the case of the gain mismatch, mainly the outer sub-carriers, while for the timing mismatch more the central sub-carriers are disturbed. Nevertheless, both results demonstrate that a much larger part of the sub-carriers is distorted by the interference component introduced by the gain and timing mismatch, compared to the case of the offset mismatch. Hence, when this interference component becomes the dominating contribution, which will happen if the number of sub-ADCs increases, or when the level of the mismatches increases, we expect that it will introduce a BER floor that is much higher than that for the offset mismatch.

Next, we present the influence of the mismatches on the BER performance. The BER results from Fig. 5 are obtained by transmitting 4-QAM modulated data symbols in 2000 OFDM symbols over an AWGN channel. The different BER curves in each of the sub-graphs correspond to L = 2, 4 and 8 sub-ADCs. The mismatches considered for the production of the BER graphs are selected as the first 2, 4 or 8 values for each mismatch in Table I, respectively. As expected, in the case of the offset mismatch, the BER curves from Fig. 5a show error floors. Based on (25), the expected values for these error floors are approximated by 1.5x10^{-4} for 2 sub-ADCs (L_1 = 1), 7.4x10^{-4} for 4 sub-ADCs (L_1 = 3) and 1.9x10^{-3} for 8 sub-ADCs (L_1 = 7), respectively. As can be observed from Fig. 5a, the error floors of the simulated BER curves are close to these theoretical approximations. Hence, (25) can easily be used to predict the performance of the OFDM system in the presence of a sufficiently large offset mismatch. Furthermore, the effects of the gain mismatch and the timing mismatch on the BER performance are presented in Fig. 5b and Fig. 5c, respectively. As can be observed, no error floor occurs for 2 sub-ADCs, although the BER performance is strongly degraded by the presence of the gain and timing mismatch, but when the number of sub-ADCs increases, a large part of the DFT outputs will be affected by an interference term, resulting in the error floor observed in the figure. Comparing Fig. 5b and Fig. 5c, the effect of the timing mismatch is larger than that of the gain mismatch. This could also be observed in Fig. 4 where the level of the interference contribution is larger for the timing mismatch than for the gain mismatch. For both cases, the level of the error floor is much higher than

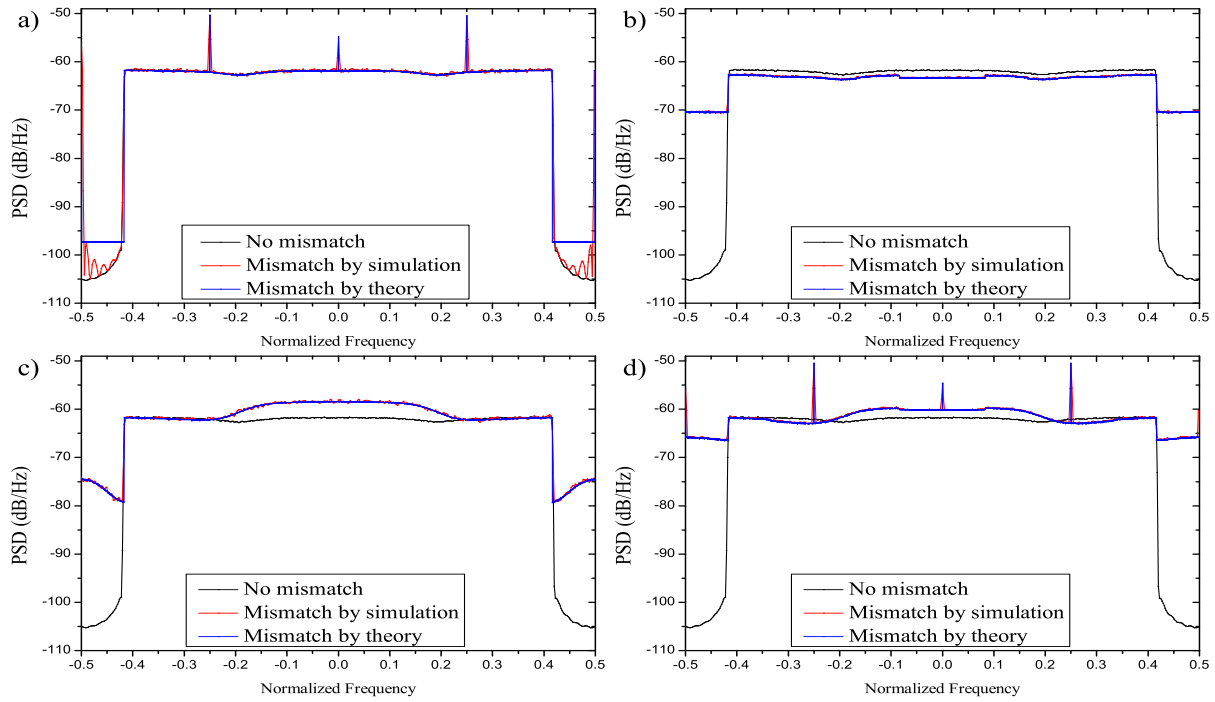

Fig. 3. The OFDM spectrum of the TI-ADC output with frequency normalized to $\frac{1}{T_s}$ and 10% mismatch level, in the presence of: a) Offset mismatch, b) Gain mismatch, c) Timing mismatch, d) Joint mismatch.

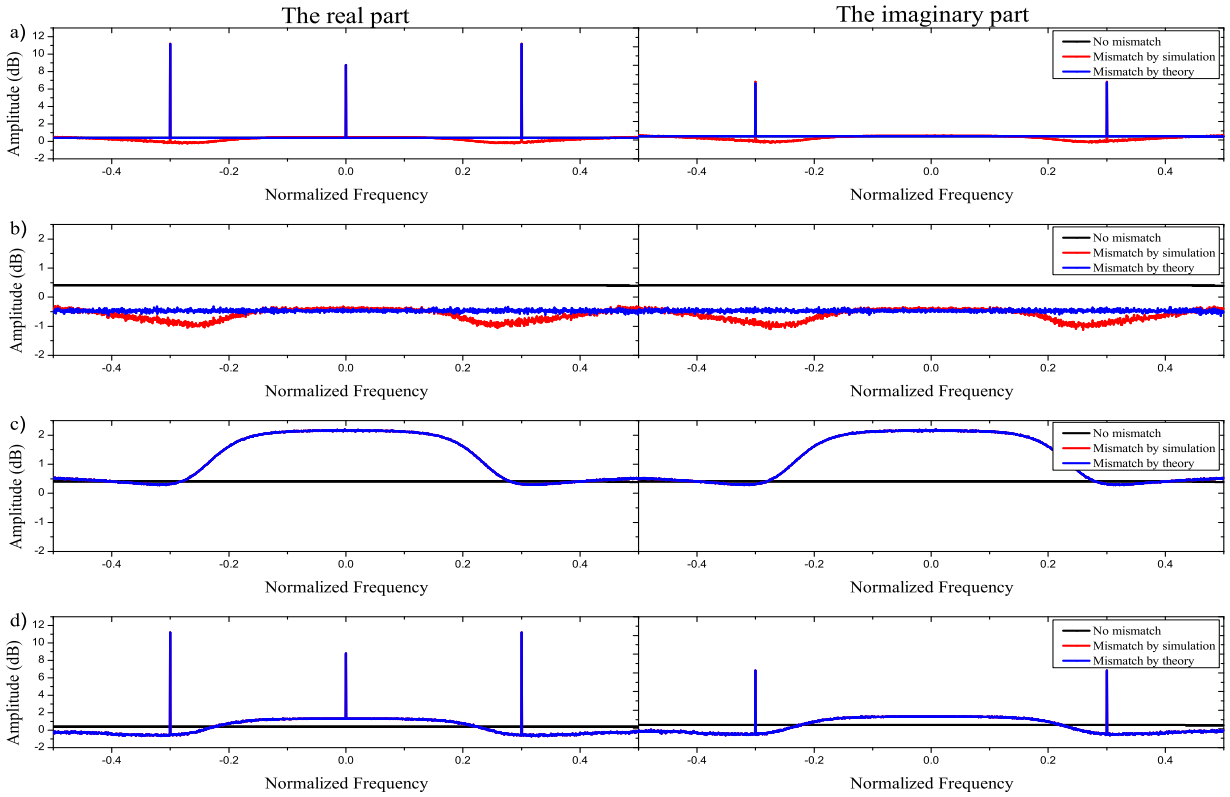

Fig. 4. The real part and the imaginary part of the DFT output with frequency normalized to $\frac{1}{T_s}$ and 10% mismatch level, in the presence of: a) Offset mismatch, b) Gain mismatch, c) Timing mismatch, d) Joint Mismatch.

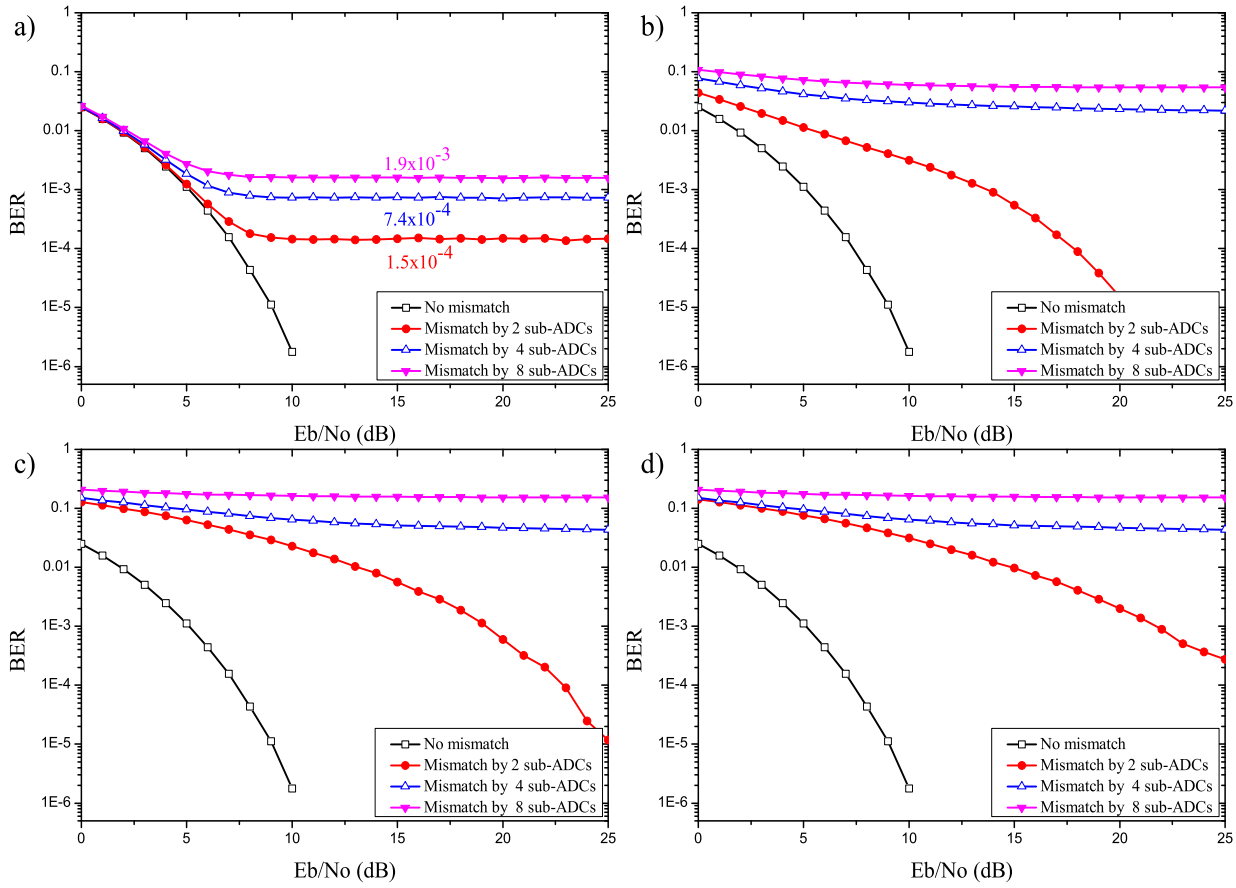

Fig. 5. BER versus Eb/No with 10% mismatch level, in the case of: a) Offset mismatch, b) Gain mismatch, c) Timing mismatch, d) Joint mismatch. The numbers in Fig. 5a are the theoretical error floor values obtained with (25)

for the offset mismatch. This can be explained as a larger part of the DFT outputs will be affected by interference, although for the offset mismatch, the few sub-carriers that are affected by the offset mismatch experience a higher interference level, as can be seen in Fig. 4d. Furthermore, for all mismatches, we observe that the BER degradation increases when the number of sub-ADCs increases. The dominating effect is the timing mismatch, as can be seen from Fig. 5d.

Up to now, we have evaluated the effect of the different mismatches for a fixed level of the mismatches, corresponding to 10% of the signal amplitude (for the offset and gain mismatch) and 10% of the sampling rate (for the timing mismatch). Next, we will consider the effect of the level of the mismatches on the performance. Fig. 6 shows the BER performance for the joint mismatch effect in the case of 4 sub-ADCs with three mismatch settings of 10%, 5% and 1%. For these later two cases, we simply scale the reference values in Table I by a factor $\frac{1}{2}$ and $\frac{1}{10}$, respectively. As can be observed in Fig. 6, the cases of 1% mismatch and 5% mismatch do not exhibit an error floor. This indicates that the offset mismatch introduces an interference term that is sufficiently small to not induce the error floor given in (25). In addition, also the interference terms caused by gain and timing mismatch do not cause an interference that gives rise to an error floor, in contrast with the case of the 10% mismatch level. However, even for the case of a 1% mismatch level, the BER performance will be strongly degraded by the presence of the mismatches, indicating that even small mismatches cannot be tolerated in an OFDM system.

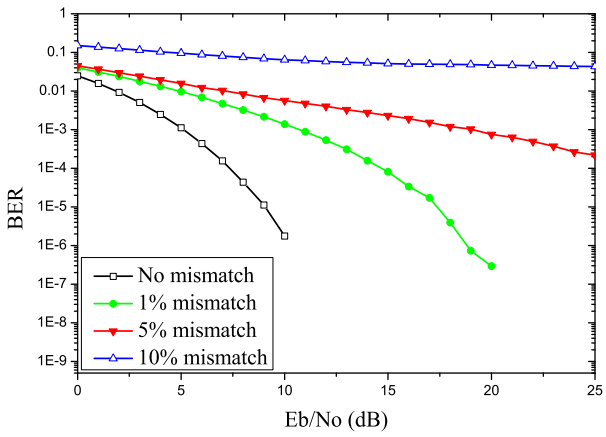

Fig. 6. BER versus Eb/No in the presence of the joint mismatch for 4 sub-ADCs with the different mismatch levels.

VI. Conclusions

High-speed sampling ADCs are considered as the bottleneck of multi-Gigabit OFDM-based systems due to the hardware limitations of current technology. An efficient approach to overcome this problem is the use of multiple parallel ADCs in a time-interleaved architecture. However, mismatches between the parallel sub-ADCs, such as offset, gain and timing mismatch can significantly degrade the system performance. In this paper, we analytically studied the influence of the TI-ADC mismatches on the spectrum and the DFT output of the OFDM system. It turns out that the evaluation of the spectrum, which is commonly used in the literature to describe the effects of the mismatches on sinusoidal signals, is not effective to study their influence on OFDM signals. Therefore, we considered the output of the DFT and the corresponding BER performance to evaluate the effects of these mismatches. The analytical expressions for the spectrum and the DFT output were compared with simulation results, and we found that our theoretical expressions are highly accurate. Hence, these expressions can be used for further investigations on the TI-ADC usage for high-speed OFDM systems.

In the case of the offset mismatch, we showed that only a few sub-carriers are affected by an interference term, that could lead to an error floor in the BER performance if the level of the mismatch is sufficiently high. A simple way to overcome this sensitivity of the OFDM system to the offset mismatch is to not modulate the sub-carriers where a peak introduced by the offset mismatch occurs. However, especially when the number of sub-ADCs further increases, such that more sub-carriers are affected by peaks, this would lead to a strong reduction in the throughput efficiency.

For the gain and timing mismatches, such a simple solution as for the offset mismatch is not available, as a much larger number of carriers is affected by an interference term. Hence, the BER degradation is much larger than for the offset mismatch. When all mismatches are present, we showed that the BER degradation increases with both the levels of the mismatches and the number of sub-ADCs, and even in the presence of a very small level of the mismatches, the BER performance strongly degrades. Hence, to overcome this problem, we will need to compensate the effects of the mismatches, either by using hardware-compensated TI-ADCs, resulting in very expensive TI-ADCs, or by estimating and compensating the mismatches through DSP, which would allow the usage of low-cost TI-ADCs.

VII. Acknowledgement

The first author gratefully acknowledges the European Commission for his Erasmus Mundus scholarship. This research has been funded by the Interuniversity Attraction Poles Programme initiated by the Belgian Science Policy Office. The authors would like to thank Prof. Ken Poulton for the helpful discussions.

References

[1] W. Shieh et al., *Orthogonal Frequency Division Multiplexing for Optical Communications*, Academic Press, USA, 2009.

[2] S. Ponnuru et al., *Joint Mismatch and Channel Compensation for High-Speed OFDM Receivers with Time-Interleaved ADCs*, IEEE Transaction on Communications, vol. 58, no. 8, 2010.

[3] Ken Poulton, *Time-Interleaved ADCs, Past and Future*, IEEE International Solid State Circuits Conference, February 10, 2009

[4] Y. Zheng et al., *DC Offset Mismatch Calibration for Time-Interleaved ADCs in High-Speed OFDM Receivers*, CCIS 337, Springer, pp. 221-230, 2013.

[5] L. Yang et al., *Oversampling to Reduce the Effect of Timing Jitter on High Speed OFDM Systems*, IEEE Communications Letters, vol. 14, no. 3, March 2010.

[6] K. N. Manoj et al., *The effect of sampling jitter in OFDM systems*, IEEE International Conference on Communications, vol. 3, pp. 2061-2065, May 2013

[7] J. Elbornsson et al., *Analysis of Mismatch Effects in a Randomly Interleaved A/D Converter System*, IEEE Transactions on Circuit and Systems, vol. 52, no. 3, 2005.

[8] ETS 300 744, *Digital broadcasting systems for television, sound and data services; framing structure, channel coding, and modulation for digital terrestrial television*, European Telecommunications Standard, DOC. 300 744, 1779

[9] P. D. Welch, *The Use of Fast Fourier Transform for The Estimation of Power Spectra: A Method Based on Time Averaging Over Short, Modified Periodograms*, IEEE Transactions on Audio and Electroacoustics, vol. AU-15, pp. 70-73, 1967.